Hindawi
Geofluids
Volume 2021, Article ID 3621040, 12 pages
https://doi.org/10.1155/2021/3621040

Research Article

Study on Influence of Joint Distribution on Surrounding Rock Failure of an Underground Tunnel

Wanrong Liu,[1,2] **Chao Peng**,[1] **and Baoliang Zhang**[1]

[1]*School of Architecture & Civil Engineering, Liaocheng University, Liaocheng, Shandong 252059, China*
[2]*State Key Laboratory of Mining Response and Disaster Prevention and Control in Deep Coal Mine, Anhui University of Science and Technology, Huainan 232001, China*

Correspondence should be addressed to Wanrong Liu; wanrongliu1989@163.com

Received 29 August 2021; Accepted 27 September 2021; Published 12 October 2021

Academic Editor: Zhijie Wen

Due to geological structure and artificial disturbance, a large number of joints and fissures are formed in the surrounding rock of an underground tunnel. In order to study the influence of joints on the failure characteristics of tunnels, three test schemes with different joint lengths, joint spacing, and joint positions are designed. The results show that the bearing capacity of the tunnel decreases with the increase in the joint length. With the increase in joint spacing, the bearing capacity of the tunnel decreases first and then increases. The crack propagation law of the three test schemes has experienced four stages: no crack, crack initiation, crack rapid development, and crack gradual reduction. The location of joints has the greatest influence on the failure mode of the tunnel. The crack is most likely to appear at the top of the tunnel and expand along the joint, mainly because it is easy to form tensile stress at the top of the tunnel and compressive stress concentration at the joint tip. Therefore, when excavating the tunnel in the underground space, the influence of joints on the tunnel should be considered. Analyzing the relationship between the tunnel and joints has important practical guiding significance for the control of the surrounding rock of the tunnel. Finally, the failure results of the indoor physical model and numerical model are compared and analyzed. They are in good agreement, which also reflects the rationality of numerical simulation.

1. Introduction

With the development of urban population and economy, the utilization of underground space is increasing day by day, and underground engineering is developing on a large scale. Working in an underground space is mainly aimed at rock mass materials. A large number of joints and fissures are formed in underground rock mass due to geological structure and artificial disturbance. As we all know, joints and fissures as weak planes directly affect the failure characteristics of rock mass. Therefore, when excavating a tunnel in an underground space, it is necessary to consider the influence of joints on the tunnel. Analyzing the position relationship between the tunnel and joints has important practical guiding significance for mastering the failure characteristics of the tunnel and controlling the surrounding rock of the tunnel.

At present, there have been many achievements in the research of jointed rock mass. Yang et al. [1] analyzed the influence of two groups of joints on the failure of rock mass materials by using artificial rock materials. The anisotropy of failure strength of rock mass was obtained. Bahaaddini et al. [2] studied the influence of discontinuous joints on the mechanical parameters of rock mass. The results show that the failure mode of rock mass is mainly determined by the joint direction and step angle, and the joint dip angle is the parameter that has the greatest influence on the properties of rock mass. Lin et al. [3] conducted uniaxial compression tests on physical model samples with different angles of columnar joints and analyzed the strength characteristics and deformation modulus of columnar jointed rock mass. Yang et al. [4, 5] analyzed the failure characteristics and crack propagation law of discontinuous jointed rock mass with holes. The influence law of joints on mechanical properties of rock mass is obtained. In the underground tunnel research, on the one hand, the deformation and failure of surrounding rock are analyzed by using the theory of

elastic-plastic mechanics, and the laws of stress and displacement of surrounding rock are studied [6]. Then it provides a theoretical basis for the support control of surrounding rock. On the other hand, the deformation and failure of jointed tunnels are studied. For example, the influence of blasting on the failure of tunnel surrounding rock [7], the damage mechanics, and the elastic-plastic mechanics considering joints are introduced to solve the surrounding rock [8, 9], and the stability of tunnel surrounding rock is studied by the block theory and numerical simulation method [10, 11]. Jia et al. and Wang et al. [12, 13] studied the failure mechanical characteristics of coal and rock mass by an acoustic emission test and analyzed the internal failure process of coal and rock mass by an acoustic emission signal. Jia and Tang [14] used RFPA software to study the effects of layered joint inclination and lateral pressure coefficient on the stability of a jointed rock tunnel. Hu et al. [15] studied the effects of different parameters such as lateral pressure coefficient, joint inclination, and joint spacing on joint parameters and lining performance by experimental and numerical simulation methods. In conclusion, there are few studies on the influence of joint distribution on tunnel failure. There is a lack of systematic research on the damage of joint distribution to the tunnel.

Based on the above research, in this paper, the numerical simulation method is used to systematically study the jointed rock tunnel, three joint distribution schemes are designed, and the effects of different joint distribution forms on the bearing capacity, crack propagation, and failure model of the tunnel are analyzed, respectively. Finally, the numerical simulation results and indoor test results are compared and analyzed. The research content is of great significance for understanding the failure of the tunnel and guiding engineering practice.

2. Test Schemes

2.1. Particle Flow Code (PFC) Theory and Parameter Checking. In order to analyze the influence characteristics of different joint forms on the failure of tunnel surrounding rock, particle flow code (PFC) is used to study it. The basic principles of a discrete element are force displacement law and Newton's second law [16]. PFC provides a PB model to bond dispersion particles. When the external force exceeds the PB bond strength between particles, the bond between particles is destroyed and the bond fracture forms microcracks. A large number of cracks gather and penetrate, resulting in macrodamage of the material. Sandstone is a typical cement material, and the failure of rock is also the place where the bond is weak. The failure process of the whole rock material is similar to that of the PB model. Therefore, the PB model can well realize the simulation analysis of rock materials. Through the built-in fish language, PFC can not only count the number of damaged microcracks but also display whether they are tensile cracks or shear cracks. It can more intuitively reflect the failure characteristics of rock. A particle discrete element has been widely used in many fields since it was proposed. In particular, a large number of research achievements have been made in geotechnical engineering [17–22]. Obtaining particle parameters is the key to PFC simulation. The microscopic parameters of particles do not correspond to the physical parameters completely, but there is a great correlation. The stiffness ratio mainly affects Poisson's ratio of rock materials, the parallel bond tensile strength mainly affects the tensile strength of materials, and the parallel bond cohesive force mainly affects the compressive strength of materials. A contact module of the particle and parallel bond deformation module jointly affect the elastic modulus of the material. Density is basically the actual density of the material. Therefore, the microparameters of PFC rock models are calibrated by simulating the uniaxial compression experiments. At present, the particle parameters are mainly obtained through a trial and error test, and the parameters of the numerical model are continuously adjusted until the numerical simulation results are consistent with the indoor test results. Finally, the indoor test and numerical simulation results are shown in Figure 1, and the particle microparameters are shown in Table 1 [23].

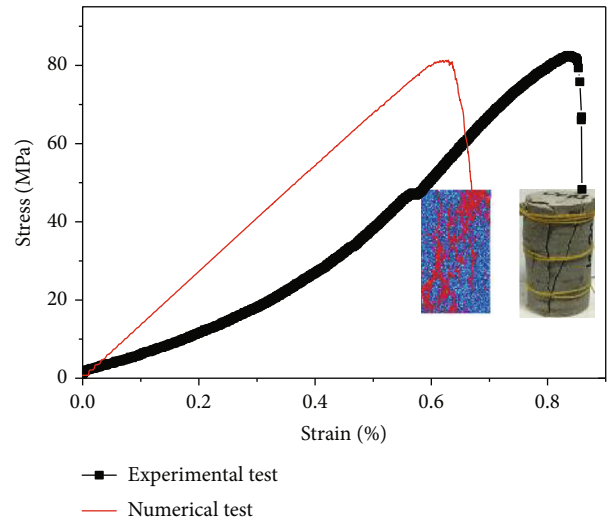

Figure 1: Stress-strain curves of sandstone based on experimental and numerical tests [23].

2.2. Test Schemes. Due to the influence of geological structure and other factors, the distribution of joints in the surrounding rock of the tunnel is complex. In the process of tunnel excavation, the tunnel and joints form different positional relations. In order to systematically explore the influence law of joints on tunnel failure, the influence of three joint distribution modes on tunnel failure is considered. The size of these tunnel models is 200 mm (width) × 200 mm (height). Due to the increase in the model scale, the diameter of particles is appropriately enlarged in order to reduce the amount of computer calculation. The minimum particle diameter is 0.8 mm, and the maximum particle diameter is 1.2 mm. The particle generation process of each model is the same. After the model is generated, the microparameters are given according to Table 1. The excavation of rock mass is completed by deleting particles. The shape of the tunnel is a straight wall semicircular arch, the radius of

Table 1: Microcosmic-mechanical parameters of the model.

Parameter	Value	Parameter	Value
Minimum particle diameter (mm)	0.3	Contact bond gap (mm)	0.05
Maximum particle diameter (mm)	0.5	Density (kg/m^3)	2500
Parallel bond tensile strength (MPa)	22	Contact modulus of the particle (GPa)	10.2
Parallel bond cohesive force (MPa)	56.5	Parallel bond deformation modulus (GPa)	16.2
Stiffness ratio	1.51	Porosity	0.1

Table 2: Mechanical parameters of the joint.

Parameter	Value	Parameter	Value
sj_kn (GPa)	1	sj_fric	30
sj_ks (GPa)	0.5	sj_coh	0
sj_large	1	sj_ten	0

the circular arch of the tunnel is 25 mm, and the size of the straight wall is 50 mm (width) × 25 mm (height). Joints are added after the tunnel excavation, and the joints form different positional relationships with the tunnel. The mechanical parameters of joints are shown in Table 2. The three schemes are different joint lengths, the distance between the joint and the tunnel, and the positional relationship between the joint and the tunnel.

2.2.1. Different Joint Length Models. In order to study the influence of borehole length on the tunnel surrounding rock mass failure, tunnel models with the joint were established (as shown in Figure 2) and the joint lengths are considered 10 mm, 20 mm, 30 mm, 40 mm, and 50 mm, respectively. The joint is located at the foot of the tunnel. And each corresponding model is abbreviated as L-10, L-20, L-30, L-40, and L-50.

2.2.2. Different Spacing between Joints and Tunnel Models. In order to study the influence of joint spacing on tunnel surrounding rock mass failure, tunnel models with different joint spacing were established (as shown in Figure 3) and the spacing is considered 0 mm, 10 mm, 20 mm, 30 mm, 40 mm, and 50 mm, respectively. The joint is located at the foot of the tunnel. The joint length is 20 mm. And each corresponding model is abbreviated as S-10, S-10, S-20, S-30, S-40, and S-50.

2.2.3. Different Joint Location Models. In order to study the influence of double-joint location on the failure characteristics of tunnel surrounding rock mass, numerical models of different locations are established, as shown in Figure 4. Double-joint length is 30 mm. The joints are located in the top and shoulder (T-S), shoulder and waist (S-W), waist and foot (W-F), foot and bottom (F-B), and bottom and top (T-B), respectively.

After the joint tunnel model is built, the compression test is carried out on the model, and the load is applied to the top wall through displacement control to realize the loading of the model. The stress, strain, crack count, and failure mode of the model were monitored during the test.

3. Analysis of Test Results

3.1. Strength Characteristics

3.1.1. Effect of Joint Length on Strength. Figure 5 shows the stress-strain curve of the tunnel model with different joint lengths. It can be seen from the figure that when the tunnel has no joints (intact), the model strength is 52.53 MPa. When the joint length gradually increases from 10 mm to 50 mm, the tunnel model strength is 49.19 MPa, 46.30 MPa, 37.81 MPa, 37.07 MPa, and 33.48 MPa, respectively. With the increase in the joint length, the strength of the tunnel model decreases gradually, and the strength decreases by 6.3%, 11.8%, 28.1%, 29.4%, and 36.3%, respectively. The length of joints has a great influence on the bearing capacity of the tunnel. It is mainly because the joints belong to the weak plane structure, which reduces the bearing capacity of the tunnel. Therefore, during excavation, the tunnel shall avoid passing through long joints as far as possible.

3.1.2. Effect of Spacing between Joints and Tunnel on Strength. Figure 6 shows the stress-strain curve of the tunnel model with different joint spacing. It can be seen from the figure that when the tunnel has no joints (intact), the model strength is 52.53 MPa. When the spacing between joints and tunnel gradually increases from 0 mm to 40 mm, the tunnel model strength is 46.30 MPa, 45.23 MPa, 46.35 MPa, 48.86 MPa, and 51.07 MPa, respectively. With the increase in the spacing between joints and tunnels, the strength of the tunnel model first decreases and then increases, but the strength is still lower than that of the no-joint model. The main reason is that the joint affects the bearing capacity of the tunnel and reduces the strength of the model. With the increase in the spacing between the joint and the tunnel, the impact of the joint on the tunnel decreases until it disappears. Therefore, the tunnel shall keep a certain distance from the joint as far as possible.

3.1.3. Effect of Joint Location on Strength. Figure 7 is stress-strain curves of models with double-joint location in different positions. It can be seen from the figure that when the double joints are located at the top and shoulder of the tunnel, the model strength is 41.42 MPa; when the double joints are located at the shoulder and waist of the tunnel, the model strength is 44.93 MPa; when the double joints are located at the waist and foot of the tunnel, the model strength is 43.23 MPa; when the double joints are located at the foot and bottom of the tunnel, the model strength is 37.82 MPa; and when the double joints are located at the bottom and top of the tunnel, the model strength is 41.22 MPa. With

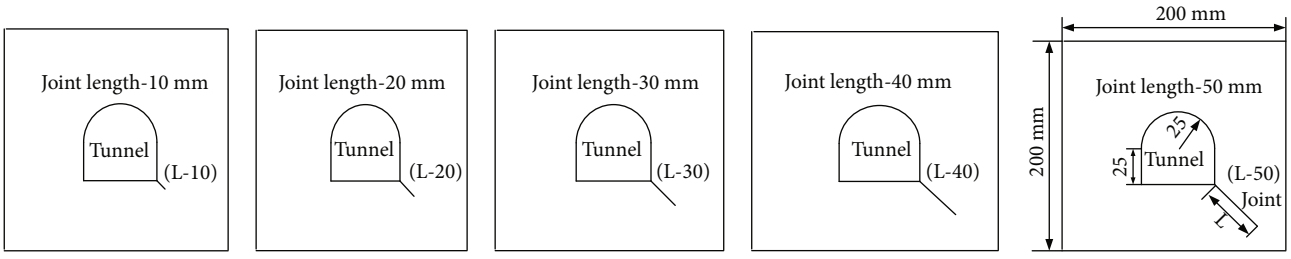

Figure 2: Different joint lengths.

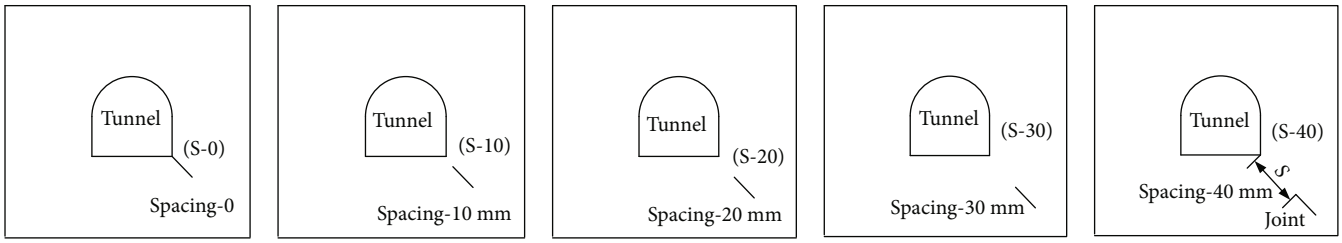

Figure 3: Different spacing between joints and tunnel.

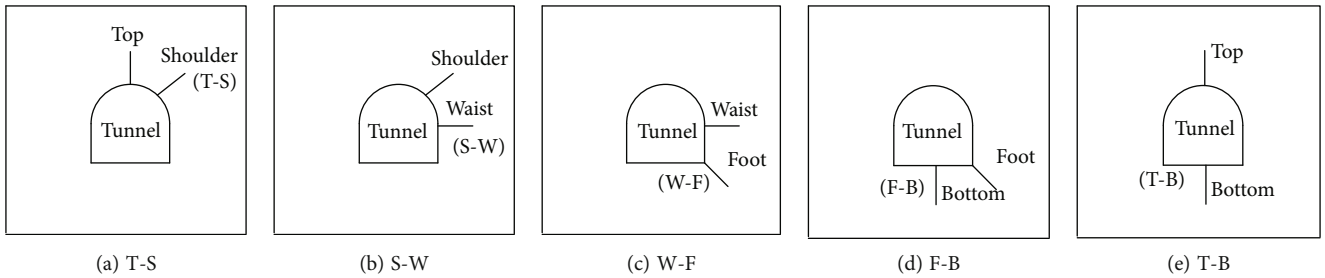

Figure 4: Double-joint location.

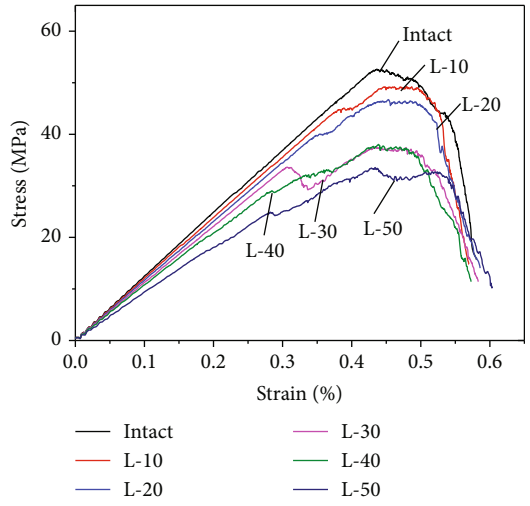

Figure 5: Stress-strain curves of models with different joint lengths.

different joint positions, the bearing capacity of the tunnel is also different. Compared with the jointless model, the bearing capacity of the tunnel is significantly reduced. Except that the bearing capacity is the lowest when the double joint is located at the bottom and foot of the tunnel, there is little difference in the bearing capacity of other models. It is mainly because the tunnel is easy to form stress concentration at the bottom corner, and 45° shear failure is easy to form due to the existence of joints. Therefore, the positional relationship between joints and tunnel should also be considered in the process of tunnel excavation.

3.2. Crack Propagation Characteristics

3.2.1. Influence of Joint Length. Figure 8 shows the stress-crack count curve of models with different joint lengths. It can be seen from Figure 8 that the distribution law of the crack count curve of each model is basically similar. The crack curves have experienced four stages: no crack, crack initiation, crack rapid development, and crack gradual reduction. For the intact model (Figure 8(a)), when the stress is 0-30.1 MPa, there is no crack (the stage of OA). When the stress exceeds 30.1 MPa, the crack begins to initiate and a certain number of cracks appear (the stage of AB). When it is close to the peak stress, the crack begins to develop and expand, and a large number of cracks gather (the stage of BC). The crack accumulation leads to the failure

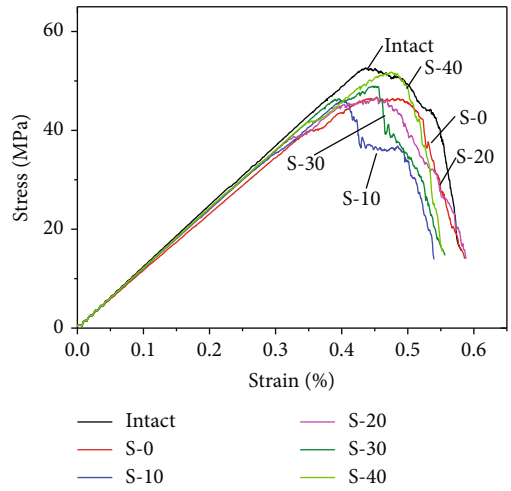

Figure 6: Stress-strain curves of models with different spacing between joints and tunnel.

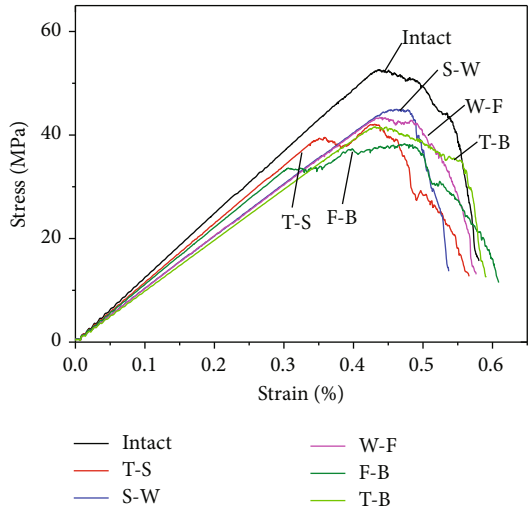

Figure 7: Stress-strain curves of models with double-joint location in different positions.

of the tunnel, the bearing capacity of the tunnel decreases, and the crack count also decreases, but a certain crack count is still maintained. Finally, the crack of the sample decreases gradually and the sample is completely destroyed (the stage of CD). For the tunnel model with joint length of 10 mm, the initiation stress is 19.6 MPa. When the strain is 0.4%, there is a small fluctuation in the stress-strain curve at the corresponding position, and the crack count increases sharply at the position of stress fluctuation. For the tunnel model with joint length of 20 mm, the initiation stress is 10.2 MPa. For the tunnel model with joint of 30 mm, the initiation stress is 11.3 MPa. When the strain is 0.33%, the stress fluctuates, mainly because the local bearing capacity decreases after the crack breaks along the joint. For the tunnel model with 40 mm joint, the initiation stress is 10.8 MPa, and for the tunnel model with 50 mm joint, the initiation stress is 10.2 MPa. Joints affect the initiation time of cracks in the surrounding rock of the tunnel. The crack distribution process reflects the failure process of the tunnel.

3.2.2. Influence of Joint Spacing between Joints and Tunnel. Figure 9 shows the stress-crack counts of models with different spacing between joints and tunnel. It can be seen from Figure 9 that the distribution law of the crack count curve is basically the same. The crack curves have experienced four stages: no crack, crack initiation, rapid crack development, and gradual crack reduction. For the jointless model, the curve law is the same as that in Figure 8(a). For the tunnel model with spacing of 0 mm, the initiation stress is 10.2 MPa, and for the tunnel model with spacing of 10 mm, the initiation stress is 20.3 MPa. For the tunnel model with spacing of 20 mm, the initiation stress is 11.8 MPa. For the tunnel model with spacing of 30 mm, the initiation stress is 20.8 MPa. For the tunnel model with spacing of 40 mm, the initiation stress is 11.5 MPa. The crack initiation time of the jointed tunnel is less than that of the no-joint tunnel.

3.2.3. Influence of Double-Joint Locations. Figure 10 shows the stress-crack counts of models with different double-joint locations. The crack distribution curve shows a similar evolution law. The crack curves have experienced a similar evolution process. When the joint is at position T-S, the crack initiation stress of the model is 14.5 MPa, and the crack counting curve has experienced three peaks. The first stress fluctuation occurs before the peak stress, which is mainly due to the crack propagation along the joint direction when the stress reaches a certain strength. The second peak stress appears at the position where the strain is 0.45%, which is mainly due to the accumulation of a large number of cracks and the sharp increase in cracks. The third time appears at the postpeak position. The initiation stress of the model at position S-W, position W-F, position F-B, and position B-T is 14.5 MPa, 12.6 MPa, 13.1 MPa, and 16.7 MPa, respectively. The model with the fastest postpeak stress drop is position S-W, and the total number of cracks is less than that of other models. The maximum crack count appears in the B-T model.

3.3. Failure Mode. The failure mode can reflect the fracture process of the tunnel, and understanding the failure of the tunnel has important guiding significance for the excavation of the tunnel. Therefore, the failure characteristics of the tunnel are analyzed below.

3.3.1. Influence of Joint Length. Figure 11 shows the failure mode of the tunnel with different joint lengths when the strength is 0.95 times the postpeak stress. In the model, the red is the crack distribution, and the black in the lower right corner is the joint. When it is an intact tunnel, the crack first starts to initiate at the top and bottom of the tunnel, and then, the crack extends along the vertical direction. At the same time, a large number of cracks also appear in the lower right corner of the tunnel and gradually penetrate. When the joint length is 10 mm, the crack first starts to sprout at the top of the tunnel and the joint position; then, the top crack extends along the vertical direction, and the crack at the joint extends downward along the vertical direction of the

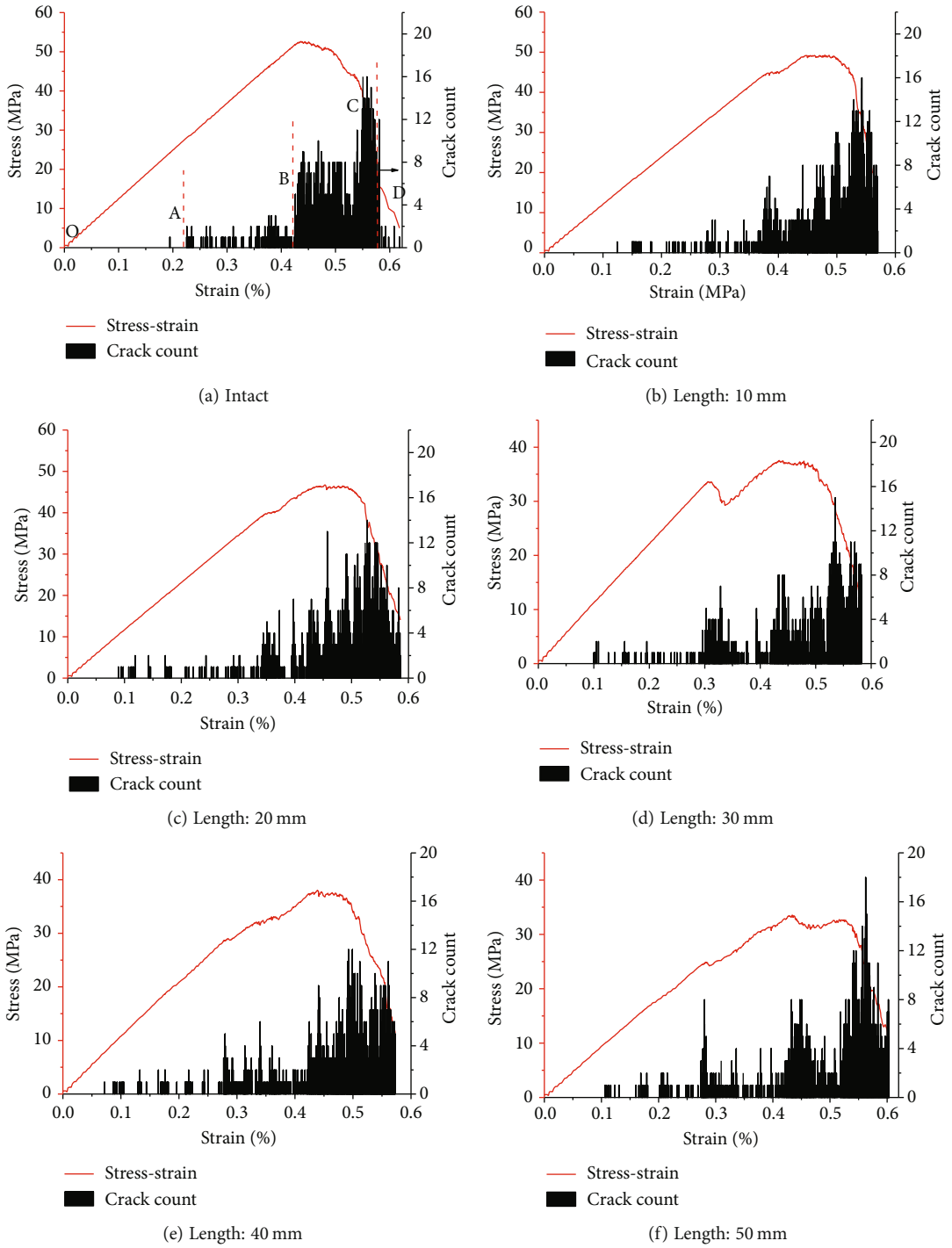

Figure 8: Stress-crack count curve of models with different joint lengths.

joint. At the same time, there are cracks on the left and right sides of the model. When the joint length is 20 mm, the crack first starts to sprout at the top of the tunnel and the joint position; then, the top crack extends along the vertical direction, and the crack at the joint extends downward along the vertical direction of the joint. At the same time, the crack formed in the lower right corner of the model gradually penetrates with the joint. When the joint length is 30 mm, the crack extends along the top of the tunnel and the joint position. The top crack penetrates the tunnel upward, and an inverted V-shaped crack is formed in the lower right corner. When the joint length is 40 mm, the crack distribution is similar to that when the joint length is 30 mm, but obvious cracks appear in the arch shoulder of the tunnel, and local damage appears in the lower left corner. When the joint length is 50 mm, the crack failure starts to sprout and expand from the spandrel. The tunnel failure is mainly caused by the penetration of the crack and the joint in the

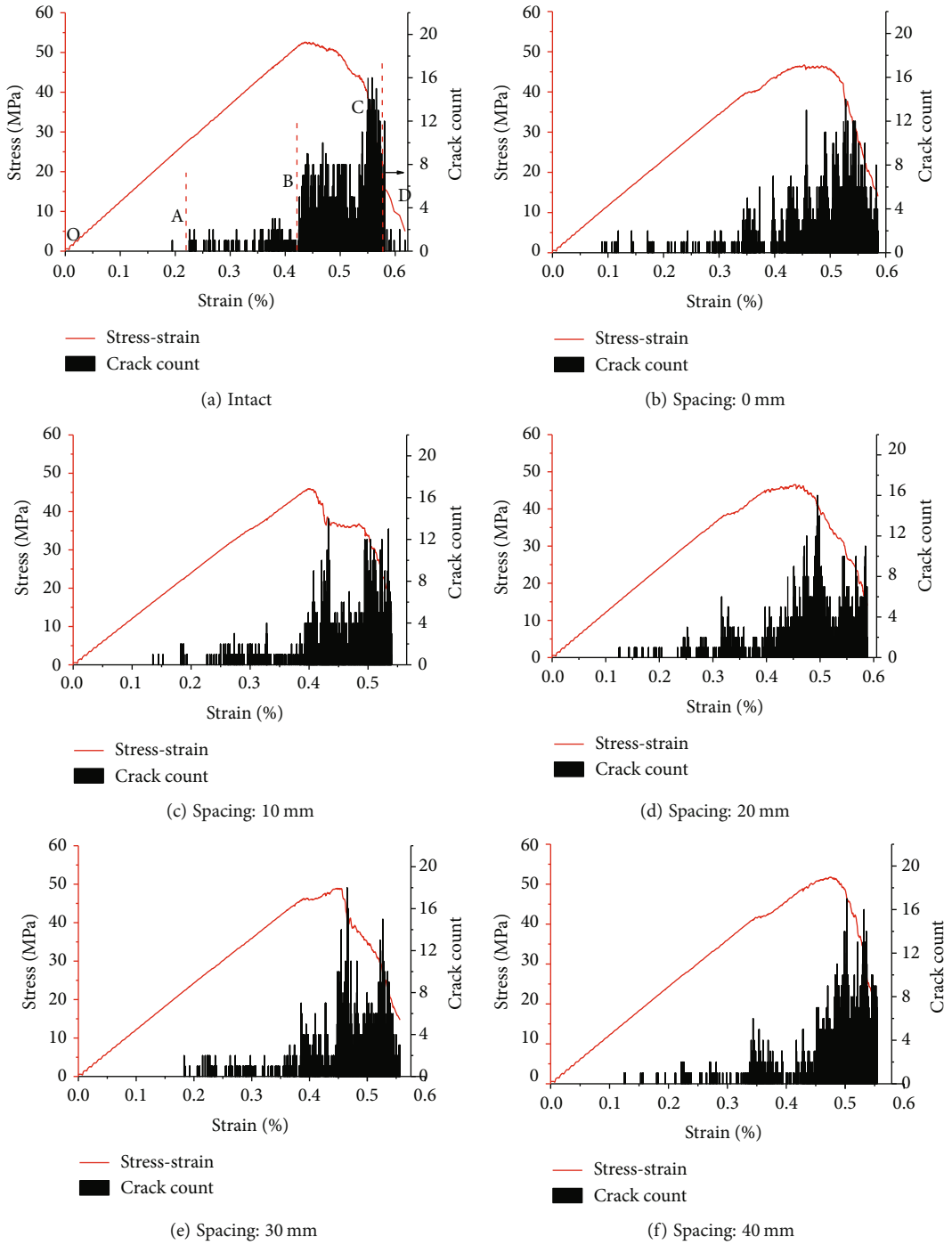

Figure 9: Stress-crack counts of models with different spacing between joints and tunnel.

lower right corner. With the increase in joint length, the failure of the tunnel is mainly concentrated in the joint position at the lower right corner, which is also the main reason for the decline of the bearing capacity of the tunnel.

3.3.2. Influence of Joint Spacing between Joints and Tunnel. Figure 12 shows the failure modes of the tunnel with different spacing between joints and tunnel. When the spacing S is 0 mm, the failure characteristics are the same as in Figure 11(c). When the spacing S is 10 mm, the crack initiates and expands along the top of the tunnel, and the crack also extends along the lower right corner of the joint to form a through crack, and the rock bridge between the tunnel and the joint is damaged. When the spacing S is 20 mm and 30 mm, some cracks also initiate and expand along the top of the tunnel, the cracks in the lower right corner extend along the joint direction, and the damage is mainly concentrated in the lower right corner. When the spacing S is 40 mm, due to the increase in the spacing between the joint and the tunnel, the crack extends along the vertical direction

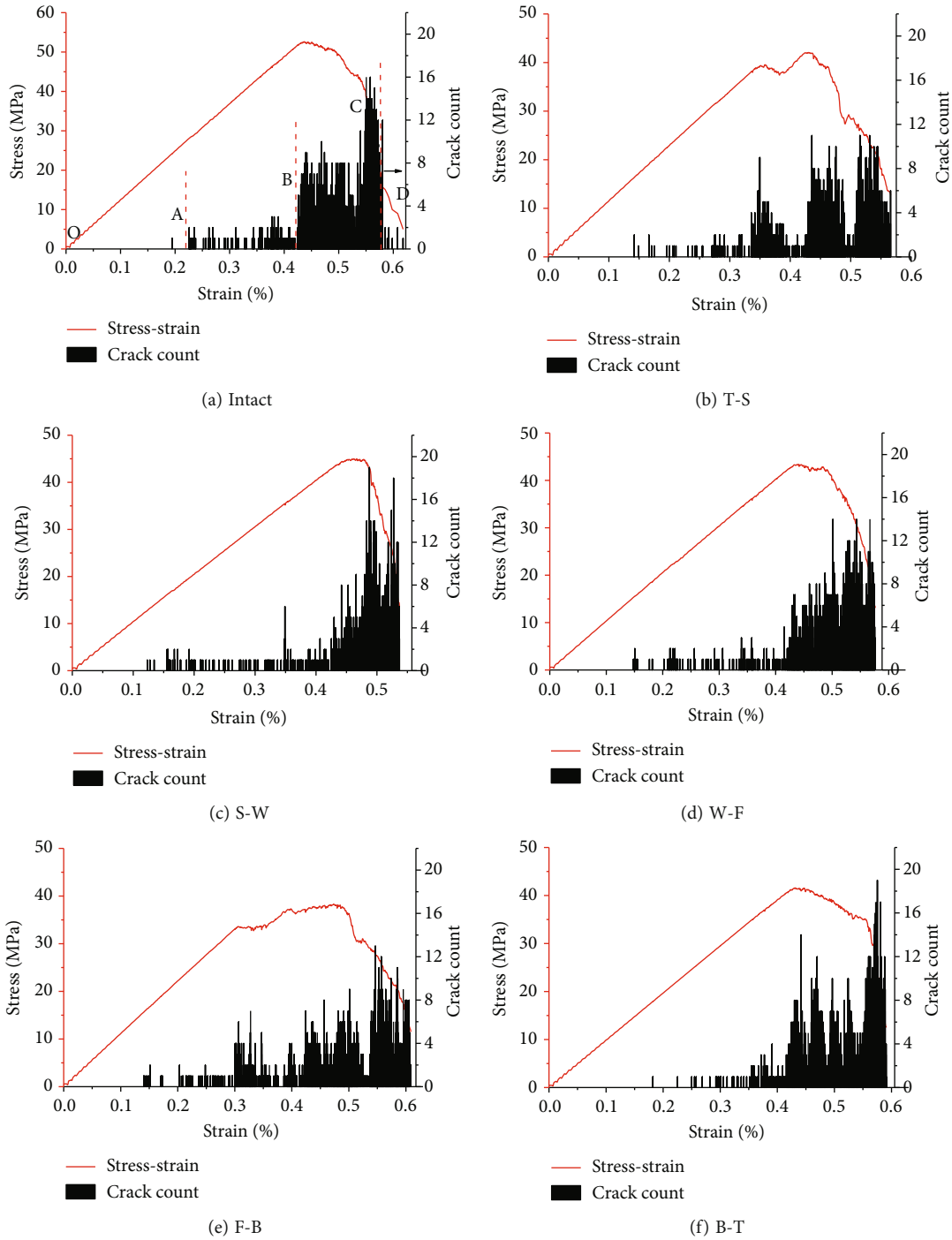

Figure 10: Stress-crack count curve of models with double-joint location.

after initiation at the joint position. The rock bridge between the joint and the tunnel has only a few cracks and is not damaged. The cracks of the whole model are mainly distributed in the upper left corner and near the joint. With the increase in spacing, the influence of joints on the tunnel decreases gradually.

3.3.3. Influence of Double-Joint Locations. Figure 13 shows the failure modes of the tunnel with different double-joint locations. When the double joints are at the position T-S, the crack propagates along the vertical direction of the top joint and the direction of the shoulder joint. Crack propagation also appeared in the lower right corner of the tunnel, mainly because it is easy to form stress concentration at the right foot of the tunnel. When the double joints are located at the position S-W, the crack also propagates along the joint direction of the shoulder and waist, but the crack propagation of the shoulder is obviously stronger than that of the waist, and local failure occurs in the lower left corner of the tunnel. When the double joints are at the position W-

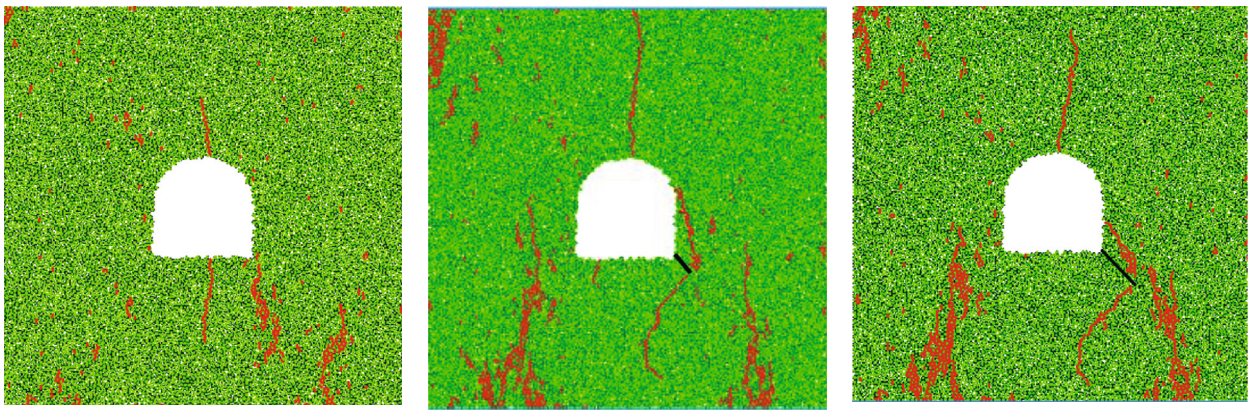

(a) Intact (b) L: 10 mm (c) L: 20 mm

(d) L: 30 mm (e) L: 40 mm (f) L: 50 mm

Figure 11: Failure modes of the tunnel with different joint lengths.

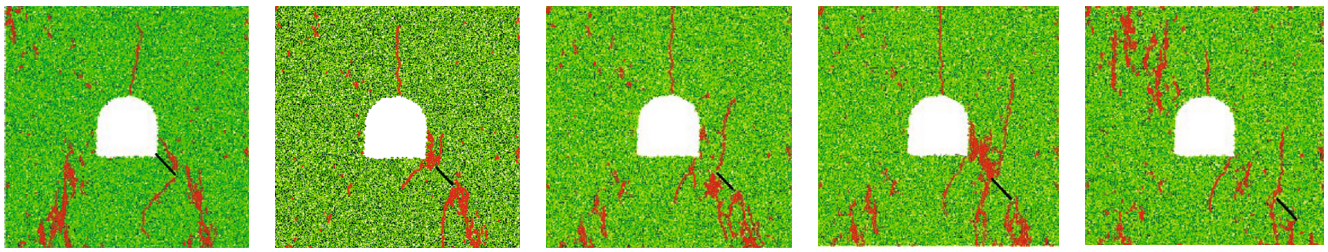

(a) S: 0 mm (b) S: 10 mm (c) S: 20 mm (d) S: 30 mm (e) S: 40 mm

Figure 12: Failure characteristics of the tunnel with different borehole spacing.

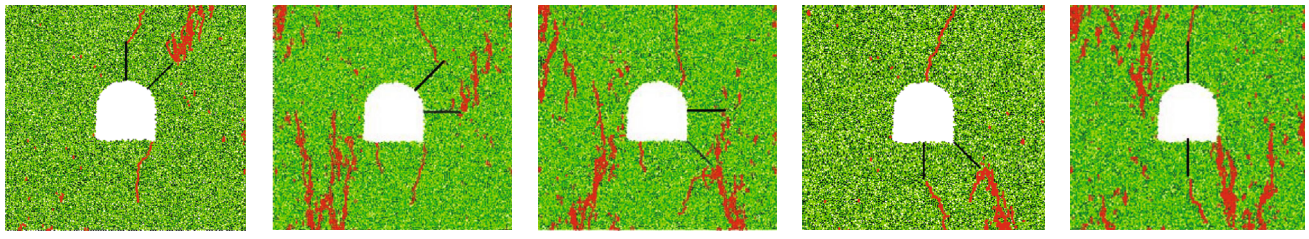

(a) T-S (b) S-W (c) W-F (d) F-B (e) T-B

Figure 13: Failure characteristics of the tunnel with different double-joint locations.

F, the crack extends vertically along the top of the tunnel, and the crack extends to the lower right corner along the joint at the foot. There are few cracks at the arch waist. It can be seen that the joints at the arch waist have little impact on the failure of the tunnel, and there is local failure on the left side of the tunnel. When the double joints are at the

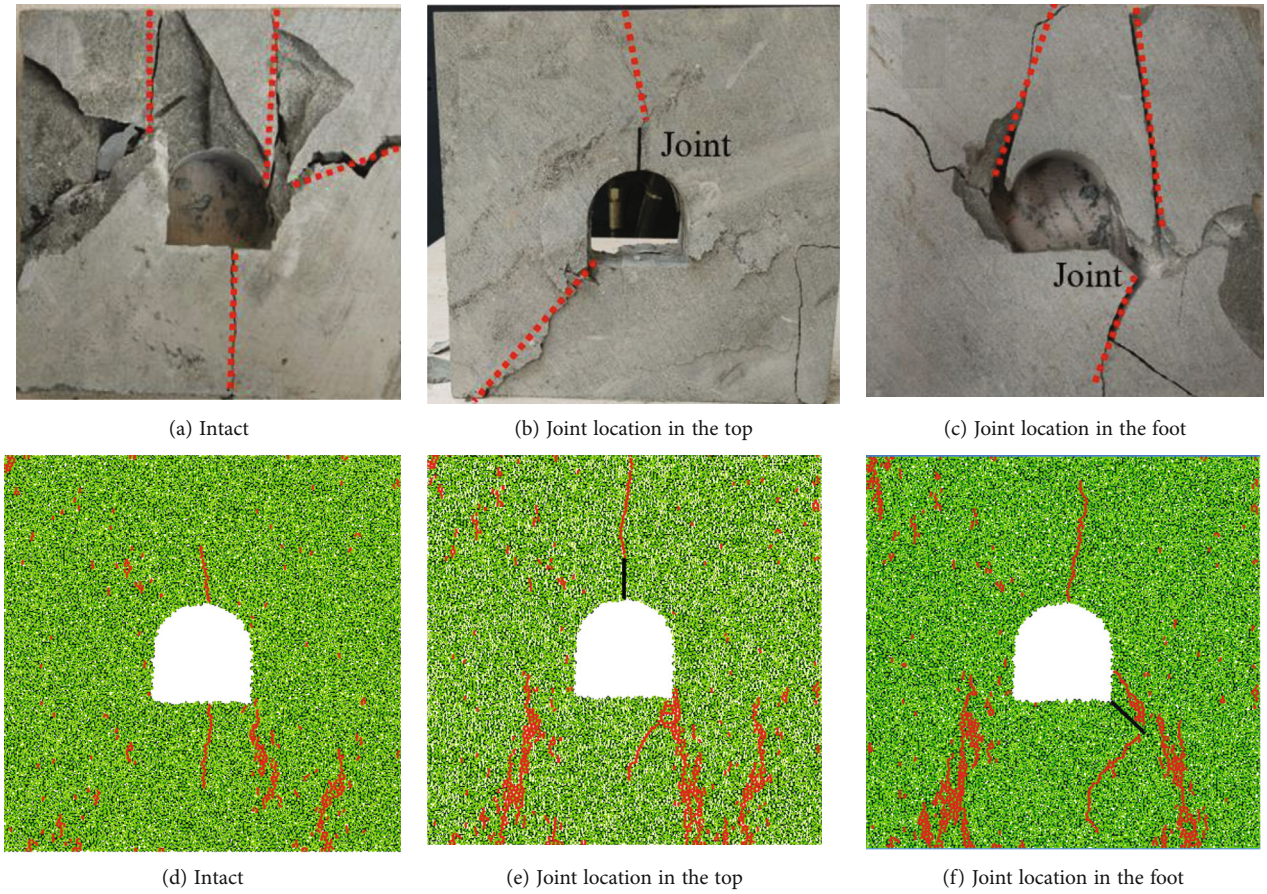

(a) Intact (b) Joint location in the top (c) Joint location in the foot

(d) Intact (e) Joint location in the top (f) Joint location in the foot

Figure 14: Experiment and numerical simulation.

position F-B, the crack extends vertically along the top of the tunnel, along the joint at the arch foot to the lower right corner, and vertically downward along the joint at the bottom. When the double joints are located at position T-B, the crack extends vertically along the top and bottom of the tunnel, and a large number of cracks appear in the local area of the tunnel. It can be seen that the existence of cracks directly affects the failure modes of the tunnel and changes the failure path of the tunnel.

4. Comparison and Discussion

Joints directly affect the failure characteristics of the surrounding rock of the tunnel. In order to further analyze the influence of joint distribution on tunnel surrounding rock, the indoor physical model mechanical test research on the jointed tunnel has been carried out, as shown in Figure 14 [24]. The size of the tunnel model is 200 mm (length) × 200 mm (height) × 50 mm (thickness). The tunnel is straight wall semicircle arch-shaped, and the radius of the semicircular arch and the length of the straight wall are both 25 mm. The joint length is 20 mm. The failure mode after the compression test of the physical model tunnel is shown in Figure 14. Figure 14(a) is the intact tunnel failure mode diagram, and Figure 14(b) is the tunnel failure mode with the joint at the top, and Figure 14(c) is the tunnel failure mode with the joint at the foot. Figures 14(d)–14(f) show the failure modes obtained from the numerical simulation results. It can be seen from the figure that the failure characteristics of both indoor experiments and numerical simulation are in good agreement. For the complete tunnel model, the failure of the tunnel is at the top and bottom, and the cracks mainly expand along the vertical direction. However, the indoor test model has obvious block spalling in the semicircular arch of the tunnel, and cracks extend to the left and right sides. For the tunnel model with joints at the top, the cracks extend vertically upward along the joint direction, and inclined downward cracks appear in the lower left corner, but some cracks also appear in the lower right corner of the numerical model. For the tunnel model with the joint at the foot, the crack first extends along the joint direction in the lower right corner, and an upward extending crack appears at the top of the tunnel. However, for the indoor physical model, the crack also extends vertically along the joint position, and for the numerical model, the crack extends along the lower left corner. The crack of the model is easy to appear at the top of the tunnel and expand along the joint position. It is mainly because it is easy to form tensile stress at the top of the tunnel and compressive stress concentration at the joint tip. Through the comparative analysis, it can be seen that the numerical simulation can better reflect the failure characteristics of the tunnel. It is reasonable to study the influence law of complex joint distribution on the failure of the tunnel by using the numerical

simulation method. Nevertheless, there is still a certain deviation between the indoor test results and the numerical simulation, and some factors need to be further considered. For example, the three-dimensional model is used in the physical test, while the numerical simulation is two-dimensional. Considering the running speed of the computer, the particle size in numerical simulation is larger than that of actual sandstone. The discreteness of actual rock failure is much larger than that of numerical simulation samples. Therefore, more influencing factors should be considered in the future research to make it more consistent with the reality.

5. Conclusion

In order to study the influence of joints on the failure characteristics of tunnels, three test schemes with different joint lengths, joint spacing, and joint positions are designed. The conclusions are as follows:

(1) The bearing capacity of the tunnel decreases with the increase in the joint length. The length of joints has a great influence on the bearing capacity of the tunnel. With the increase in joint spacing, the bearing capacity of the tunnel decreases first and then increases. With different joint positions, the bearing capacity of the tunnel is also different. When the double joint is located in B-F, the bearing capacity of the tunnel is the lowest

(2) The distribution law of the crack count curve of each model is basically similar. The crack curves have experienced four stages. In the first stage, the stress is small and there is no crack. In the second stage, cracks appear with the increase in stress. In the third stage, with the further increase in stress, a large number of cracks gather and expand. In the fourth stage, the sample is damaged and the cracks are gradually reduced

(3) With the increase in joint length, the failure of the tunnel is mainly concentrated in the joint position at the lower right corner. With the increase in spacing, the influence of joints on the tunnel decreases gradually. The existence of cracks directly affects the failure modes of the tunnel and changes the failure path of the tunnel. The crack is most likely to appear at the top of the tunnel and expand along the joint. Analyzing the relationship between the tunnel and joints has important practical guiding significance for the control of the surrounding rock of the tunnel

Data Availability

The data used to support the findings of this study are included within the article.

Conflicts of Interest

The authors declare that they have no conflicts of interest.

Acknowledgments

This study was supported by the State Key Laboratory of Mining Response and Disaster Prevention and Control in Deep Coal Mine Research Fund (SKLMRDPC20KF09), Research Project of Undergraduate Teaching Reform in Shandong Province (P2020013), and Research Fund of Liaocheng University (318051703, 318011901, and 318012014).

References

[1] Z. Y. Yang, J. M. Chen, and T. H. Huang, "Effect of joint sets on the strength and deformation of rock mass models," *International Journal of Rock Mechanics and Mining Sciences*, vol. 35, no. 1, pp. 75–84, 1998.

[2] M. Bahaaddini, G. Sharrock, and B. K. Hebblewhite, "Numerical investigation of the effect of joint geometrical parameters on the mechanical properties of a non-persistent jointed rock mass under uniaxial compression," *Computers and Geotechnics*, vol. 49, pp. 206–225, 2013.

[3] Z. Lin, W. Xu, W. Wang et al., "Determination of strength and deformation properties of columnar jointed rock mass using physical model tests," *KSCE Journal of Civil Engineering*, vol. 22, no. 9, pp. 3302–3311, 2018.

[4] X. X. Yang, H. W. Jing, C. A. Tang, and S. Q. Yang, "Effect of parallel joint interaction on mechanical behavior of jointed rock mass models," *International Journal of Rock Mechanics and Mining Sciences*, vol. 92, pp. 40–53, 2017.

[5] S. Q. Yang, P. F. Yin, Y. C. Zhang et al., "Failure behavior and crack evolution mechanism of a non-persistent jointed rock mass containing a circular hole," *International Journal of Rock Mechanics and Mining Sciences*, vol. 114, pp. 101–121, 2019.

[6] A. Singh, K. Seshagiri Rao, and R. Ayothiraman, "A closed-form analytical solution for circular opening in rocks using Drucker–Prager criterion," *Indian Geotechnical Journal*, vol. 49, no. 4, pp. 437–454, 2019.

[7] S. Kuili and V. R. Sastry, "A numerical modelling approach to assess the behaviour of underground cavern subjected to blast loads," *International Journal of Mining Science and Technology*, vol. 28, no. 6, pp. 975–983, 2018.

[8] M. B. Wang and G. Wang, "A stress-displacement solution for a pressure tunnel with impermeable liner in elastic porous media," *Latin American Journal of Solids and Structures*, vol. 9, no. 1, pp. 95–110, 2012.

[9] W. Yang, Q. Zhang, P. G. Ranjith et al., "A damage mechanical model applied to analysis of mechanical properties of jointed rock masses," *Tunnelling and Underground Space Technology*, vol. 84, pp. 113–128, 2019.

[10] C. Jia, Y. Li, M. Lian, and X. Zhou, "Jointed surrounding rock mass stability analysis on an underground cavern in a hydropower station based on the extended key block theory," *Energies*, vol. 10, no. 4, pp. 563–574, 2017.

[11] D. Q. Kong, C. S. Qiao, and G. C. Xue, "Stability evaluation of flat large-span cavern in jointed rock mass," *Arabian Journal of Geosciences*, vol. 13, no. 11, pp. 1–14, 2020.

[12] Z. Jia, H. Xie, R. Zhang et al., "Acoustic emission characteristics and damage evolution of coal at different depths under triaxial compression," *Rock Mechanics and Rock Engineering*, vol. 53, no. 5, pp. 2063–2076, 2020.

[13] X. Wang, Z. Wen, Y. Jiang, and H. Huang, "Experimental study on mechanical and acoustic emission characteristics of

rock-like material under non-uniformly distributed loads," *Rock Mechanics and Rock Engineering*, vol. 51, no. 3, pp. 729–745, 2018.

[14] P. Jia and C. A. Tang, "Numerical study on failure mechanism of tunnel in jointed rock mass," *Tunnelling and Underground Space Technology*, vol. 23, no. 5, pp. 500–507, 2008.

[15] X. Hu, Y. Fang, G. Walton, and C. He, "Experimental analysis of shield TBM tunnel lining mechanical behaviour in an anisotropically-jointed rock mass," *KSCE Journal of Civil Engineering*, vol. 23, no. 6, pp. 2733–2745, 2019.

[16] Itasca Consulting Group, *PFC Users' Manual (Version 5.0)*, Itasca, Minneapolis, MN, USA, 2014.

[17] B. An and D. D. Tannant, "Discrete element method contact model for dynamic simulation of inelastic rock impact," *Computers & Geosciences*, vol. 33, no. 4, pp. 513–521, 2017.

[18] W. Liu, J. K. Liu, and C. Zhu, "Multi-scale effect of acoustic emission characteristics of 3D rock damage," *Arabian Journal of Geosciences*, vol. 12, no. 22, 2019.

[19] S. Pourmand, H. Chakeri, M. Sharghi, and Y. Ozcelik, "Investigation of soil conditioning tests with three-dimensional numerical modeling," *Geotechnical and Geological Engineering*, vol. 36, no. 5, pp. 2869–2879, 2018.

[20] R. Yoshinaka, M. Osada, H. Park, T. Sasaki, and K. Sasaki, "Practical determination of mechanical design parameters of intact rock considering scale effect," *Engineering Geology*, vol. 96, no. 3-4, pp. 173–186, 2018.

[21] U. Castro-Filgueira, L. R. Alejano, J. Arzúa, and D. M. Ivars, "Sensitivity analysis of the micro-parameters used in a PFC analysis towards the mechanical properties of rocks," *Procedia Engineering*, vol. 191, pp. 488–495, 2017.

[22] X. Zhang and L. N. Y. Wong, "Cracking processes in rock-like material containing a single flaw under uniaxial compression: a numerical study based on parallel bonded-particle model approach," *Rock Mechanics and Rock Engineering*, vol. 45, no. 5, pp. 711–737, 2012.

[23] C. Peng and W. Liu, "Study on pressure relief effect of rock mass with different borehole parameters," *Advances in Civil Engineering*, vol. 2021, Article ID 5558673, 15 pages, 2021.

[24] W. Liu, J. Xu, Z. Wang, and C. Peng, "Experimental research on damage characteristics and safety damage threshold of jointed caverns based on acoustic emissions," *Geomechanics and Geophysics for Geo-Energy and Geo-Resources*, vol. 7, no. 3, pp. 1–14, 2021.